Ultrafast VCSEL-based plasmonic polymerase chain reaction with real-time label-free amplicon detection for point-of-care diagnostics

P.Mohammadyousef[a], G.Uchehara[a] , M.Paliouras[b], M.Trifiro[b], A.G.Kirk[a]
[a]Electrical and Computer Engineering Dept., McGill University, 3480 Rue University, Montréal, QC, H3A 2K6, Canada; [b]Lady Davis Inst. for Medical Research, Jewish General Hospital, 3755 Chemin de la Côte-Sainte-Catherine, Montréal, QC, H3T 1E2, Canada

ABSTRACT

Recent progress in microfluidics and optical systems has made enormous impact in the advancement of nucleic acid amplification and detection. However, commercial and currently reported microfluidic PCR devices have not yet found their utilization in point-of-care (POC) applications. This is due to long amplification time, high power requirement, and bulky size of commercial PCR machines or cost-inefficiency, complex fabrication and operation of microfluidic chips. In this work, we present a compact PCR device in which fast amplification is accomplished by photothermal heating of gold nanorods evenly dispersed in PCR reaction by a vertical-cavity surface-emitting laser (VCSEL). This thermocycler offers sub-ten-minute amplification time for 30 thermal cycles with high temperature stability and PCR products comparable to conventional bench-top machines. The proposed device is approximately 100mm×50mm×50mm in size, and its small footprint is obtained by hardware miniaturization. Retaining conventional sample volumes (20µL) makes our device more user-friendly in terms of sample loading and capable of more sensitive amplicon detection for on-site assays. Also, its cost-effectiveness due to disposable AuNRs and inexpensive light source outweigh surface plasmon heating methods utilizing embedded Au films with limited lifetimes and other previously presented plasmonic thermocyclers.

Keywords: Polymerase chain reaction (PCR), point of care (POC), DNA, localized surface plasmon resonance (LSPR), gold nanorods (AuNRs), surface-emitting laser

1. INTRODUCTION

Point-of-care (POC) testing refers to analytical testing activities provided outside the clinical laboratory and performed by non-laboratory or medical technician personnel near the site of the patient to provide instant availability of results. This facilitates quick medical decisions and enhances healthcare outcomes. POC testing devices should be easy-to-operate, portable, and handheld electronics or molecular collection tools. It is expected that faster and more accurate POC diagnostic tests will play a significant role in expanding health care in low- and middle-income countries where diagnostic challenges exist due to poor clinical laboratory infrastructures, lack of skilled technicians, and cost constraints [1, 2]. Therefore, many studies have focused on adapting different diagnostic tests such as polymerase chain reaction (PCR) platforms to POC settings.

PCR has become the superior molecular diagnostic technique in biochemistry and molecular biology such as gene expression, forensic analysis, and pathogen detection to evaluate medical and therapeutic decision and assess cure rates [3-7]. This technique, first developed in 1985 by K. Mullis [8], relies on thermo-stable polymerase and sequential three step temperature cycling called denaturation, annealing, and elongation to generate millions of copies of specific sequences of deoxyribonucleic acid (DNA). One cycle of PCR consists of these three steps, and a complete PCR occurs in a successive 30 to 50 cycles carried out in a thermocycler. Conventional bench-top thermocyclers take greater than an hour to complete 40 cycles depending on the protocol, instrument, and reagents [9]. This long amplification time is due to thermoelectric energy conversion which generates and removes heat from PCR reaction with the consumption of electrical energy. Many industrial groups attempt to reduce the amplification time of lab-based thermocyclers such as LightCycler® 2.0 System from Roche Molecular Systems, Inc. which completes 35 cycles of PCR in 30 minutes for a 20µL sample by using hot and cold air streams in capillary tube. Other commercial thermocyclers offer faster amplification using microplates for sample volume of 2-5µL. However, these thermocyclers are bulky in size, require specifically designed tubes, and have high power consumption in the range of 200 to 800 W. Therefore, these PCR machines are confined to central laboratories. The second generation of PCR devices takes advantage of microfluidics, microelectronics, and optical systems to make PCR more compatible for POC applications. These microscale thermocyclers enable sub-minute PCRs due to employing small PCR

reaction volume as well as high surface-to-volume ratio diffusion and heat conduction [10]. The first microfluidic PCR device was demonstrated by Kopp et al. flowing PCR mixture continuously through glass-based microchannel at different temperature zones to perform three stages of PCR (denaturation, annealing, and elongation) [11]. This approach was able to thermocycle a 10μL PCR sample for 20 cycles in 90 seconds. More work was done by changing the cross-sectional size of microchannel to control the residence time fluid in each temperature zone [12, 13]. Other studies implemented a pressurizing channel between PCR microchannel to increase the pressure downstream to prevent air bubble formation which causes PCR inhibition [14, 15]. Combining laser-induced fluorescence detection within microfluidic thermocyclers further reduced the total amplification and analysis time [16]. These mentioned studies were performed with large-scale pumps to control the flow rate of PCR, which questioned the concept of miniaturization of PCR for POC diagnostics. Thus, other studies, namely Xie et al. proposed micropumps which are more compatible with PCR microfluidic devices [17, 18]. Other groups developed high-speed PCR using high absorption of an infrared (IR) laser beam or a tungsten lamp radiation by nanoliter volume of water instead of Peltier heating/cooling [19-21]. Among all these groups, Kim et al. demonstrated the fastest IR amplification of 10-30nL of PCR mixture in 3.5 min for 50 PCR cycles. Despite their short amplification time and small footprint, PCR microfluidics demands particular microfabrication of instrumentations and tools such as micropipettes, disposable PCR plates, or droplet arrays using contact printing as well as highly precise pipetting skill in nanoliter scale [22].

The third generation of PCR thermocyclers harnesses the enhanced absorption cross-section of gold nanoparticles (AuNPs) by irradiating laser at their plasmon wavelength maximum. The ultra-fast photonic PCR proposed by Son et al. specifically designed for POC settings thermocycled 10μL sample on an Au-coated poly(methyl methacrylate) well photothermally by using a 1W 447.5nm LED [23]. In their work, since light to heat conversion was restricted to the thin layer of PCR reaction on top of thin Au film, they used small sample volume for more uniform and efficient heating. The other challenge with their plasmonic instrument is the biofouling and degradation of planar gold interface due to overusing. Other studies overcame the challenges related to surface plasmon heating by using suspended gold nanorods (AuNRs) in PCR solution [24-28]. Roche et al. used a large 2W diode laser to excite AuNRs at their resonance wavelength (808nm). The nonradiative relaxation of excited AuNRs in the form of significant heat energy highly localized near the AuNRs leads to uniform heating in PCR reaction mixture. The plasmonic thermocycler was equipped with a cooling fan to complete a 30 PCR cycles in sub-minute for 10-25μL sample volume. In this paper, the plasmonic thermocycler is miniaturized by utilizing a vertical cavity surface emitting laser (VCSEL) as the heating source. Due to the compact form factor of VCSEL, it can be placed close to the PCR tube for maximum light coupling efficiency as well as uniform heating inside the PCR reaction without the need for any additional optical components. The amplification of 300 base pair (bp) *Chlamydia Trachomatis* DNA was accomplished under ten minutes for 30 PCR thermal cycles from 60 to 85°C. In addition, employing conventional PCR tubes with 20μL PCR reaction provides ease in sample loading and simplicity in design for POC diagnostics. Abundant sample volume facilitates any post-PCR manipulation. As it has been reported that larger sample volume favors lower limit of detection in real-time PCR, integration of our system with a quantitative detection method will deliver higher sensitivity in amplicon quantification [29, 30]. The AuNRs are robust in PCR solution after prolonged laser irradiation, which leads to stable temperature regulation and consistent PCR results. In contrast to other plasmonic thermocyclers with embedded Au films which need constant quality control of experiments' outcome due to degradation of Au film, AuNRs are disposable and more cost-effective. The other advantage with AuNRs is that heating rate can be altered by increasing or reducing AuNRs' concentration, whereas prefabricated Au films do not offer this flexibility in changing the heating rate. The proposed thermocycler has the potential to circumvent some of the limitations of current PCR thermocyclers with its simple, low-cost, small footprint, and large sample volume to serve as a POC diagnostic device.

2. MATERIALS AND METHODS

2.1 Plasmonic PCR Reagents

Poly(enthylene glycol)-modified gold nanorods (PEG-AuNRs) were purchased from Nanopartz (Loveland, CO). The longitudinal and transverse surface plasmon absorption peaks are at 808 and 507nm. **Figure 1** demonstrates these PEG-AuNRs under Transmission Electron Microscopy (TEM) with diameter of 10nm and aspect ratio of 4.1. The choice of near infrared 808nm AuNRs and laser heating is favorable since PCR ingredients have minimum absorption at this wavelength.

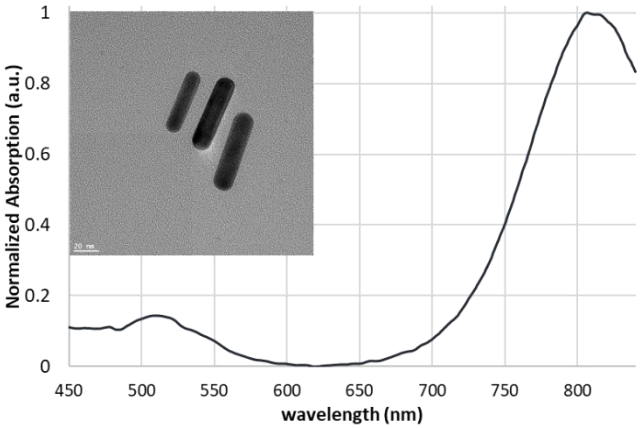

Figure 1. Absorption spectrum of PEG-AuNRs purchased from Nanopartz.

The molarity of 2.5nM for PEG-AuNRs was used as an optimal concentration for fast thermocycling as well as maximum PCR efficiency. The forward primer 5'-TCCGGAGCGAGTTACGAAGA-3'and reverse primer 5'-AATCAATGCCCGGGATTGGT-3' were chosen to amplify 4.5×10^5 copies of *Chlamydia Trachomatis* Strain LGV III purchased from (Manassas, VA). The DNA template was diluted with double distilled water (DDW) to achieve lower copy number of 10^4 for our experiments. Hemo KlenTaq, KAPA2G, and Phusion polymerases have final extension rates of 2 m, 15 s, and 15 s per 1kb. Both KlenTaq and Phusion and their buffers were purchased from New England Biolabs (Ipswich, MA), and KAPA2G was purchased from Kapa Biosystems (Wilmington, MA). The standard concentrations of ingredients followed the PCR Protocol for each enzyme. However, the concentration of PEG-AuNRs is the same regardless of polymerase type. **Table 1** demonstrates the volume and the initial concentration of PCR components with different polymerases. The 20µL PCR reaction is placed into a 0.2ml thin wall plastic tube, covered with 50µL of mineral oil, and capped. The use of mineral oil is to prevent water evaporation and any change in sample volume. Maintaining the conventional PCR sample volume and tube allows on-site sample loading and analysis with much more convenience.

Table 1. Volume of different PCR components.

PCR component	Volume (µL)
5X Taq/KAPA2G/Phusion Reaction Buffer	4
Taq/KAPA2G/Phusion polymerase	0.8/0.1/1
dNTP (2mM)	0.6
Forward Primer (5µM)	0.6
Reverse Primer (5µM)	0.6
DNA (10^4 copies)	1
PEG-AuNRs (50nM)	1
d_2H_2O	11.4
Total	20

2.2 Instrument Design

The non-contact heating is performed by an 808nm 3W vertical cavity surface-emitting laser (VCSEL) obtained from Tyson Technology Co. (Shenzhen, China). A 2A BiCMOS constant current source (STCS2A) purchased from STMicroelectronics to drive the VCSEL. The current was set to 2A by an external resistor, and the PWM dimming pin of STCS2A changes the current passing through the VCSEL for temperature regulation. One advantage of VCSEL-based thermocycler is its compact form factor which allows us to place it as close as possible to PCR tube without using any

optical components to direct light on tube. To have maximum heating rate, the laser is placed in an optimal position, so that maximum VCSEL's optical power (3W) couples into PCR tube. Using Zemax non-sequential mode, an optical design program, free-space Gaussian beam propagation was modelled to calculate the total power received by PCR solution from the light source (VCSEL). In the optical design software, the PCR solution was modelled as water, and a photodetector was placed inside the tube to trace the nonsequential rays. **Figure 2.a** shows that there is no loss in VCSEL's optical power received at photodetector's sight with 5mm separation between tube and VCSEL; however, more than 5mm separation leads to poor beam coupling and far field beam divergence (**Figure 2.b**). Therefore, the VCSEL is placed 3mm below the tube, so that the maximum beam width couples into the PCR tube's domed bottom.

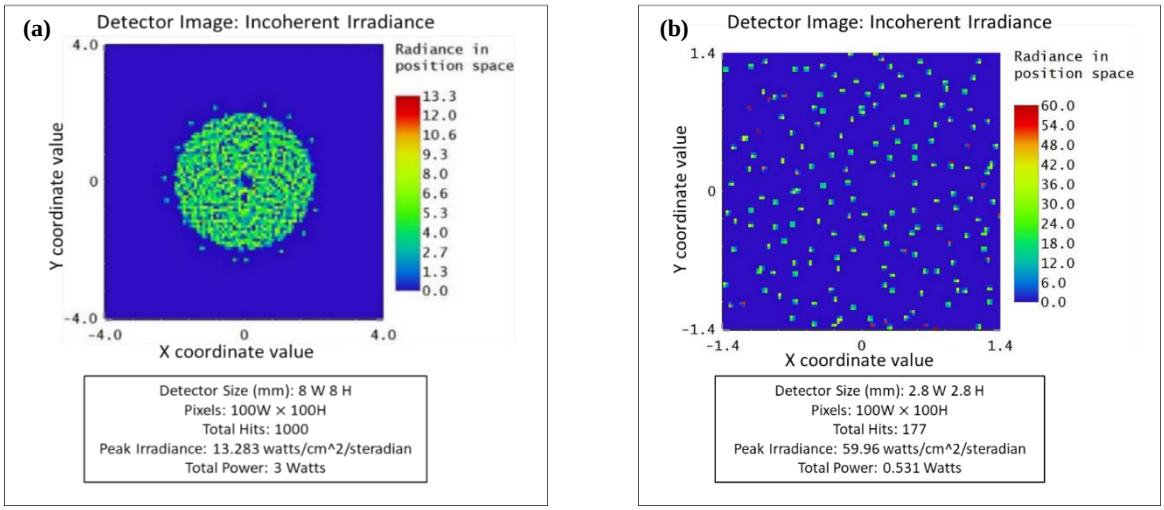

Figure 2. (**a**) Incoherent irradiance with 5mm and (**b**) 20mm VCSEL-tube separation.

A copper heatsink is attached to VCSEL to facilitate heat dissipation. It can be argued that thermal management and PCR temperature stability might be disturbed due to closely spaced VCSEL and tube. However, based on thermal images shown in **Figure 3,** the maximum temperature increase for VCSEL is 3°C when the tube's temperature fluctuates between 55 to 80°C. This confirms that heating laser has minimal to zero disturbance to temperature regulation and stability. A 14V DC brushless fan cools the tube in opposite direction of heating. Both VCSEL and fan are modulated through an Arduino microcontroller connected to PWM pin of current source and fan's switch, respectively. An infrared thermometer measures the temperature of reaction 10mm from one side of tube. The IR thermometer's emissivity and transmission were calibrated with a contact temperature probe (thermocouple). Arduino records and sends the data through USB link connected to computer. **Figure 4** shows the basic arrangement of the VCSEL-based thermocycler. The most expensive parts of this plasmonic thermocycler are the IR thermometer, VCSEL, and Arduino Microcontroller which cost 343, 68, and 38 CAD. The rest of the components, namely the fan and electronics cost less than 15 CAD. This makes our VCSEL-based device the most low-priced plasmonic thermocycler reported to date.

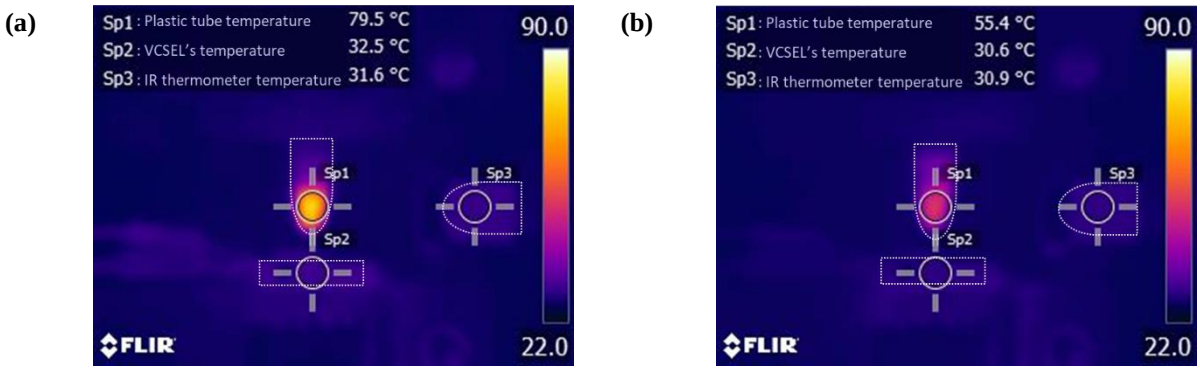

Figure 3. Thermal image and plasmonic thermocycler's components temperature close to (**a**) Denaturation and (**b**) annealing stage.

2.3 Plasmonic thermocycling

Plasmonic thermocycling is conducted using a 1s denaturation step at 85°C, a 5s annealing step at 60°C, and 1s elongation step at 72°C. The purpose of maintaining the temperatures for 1s (denaturation), 5s (annealing), and 1s (elongation) is to allow double stranded DNAs (dsDNAs) to go through melting process, primers to hybridize to the target sequences, and polymerase to extend and replicate the new DNA strands. Cycling was repeated a total of 30 times. Defined temperatures and timings are controlled by the communication between the microcontroller and computer. Arduino regulates the current of STCS2A via the PWM pin and subsequently the optical output power of VCSEL to increase or hold the temperature. The gate input voltage of a MOSFET switch is biased by Arduino; as a result, the fan as the resistive load of the switch is actuated.

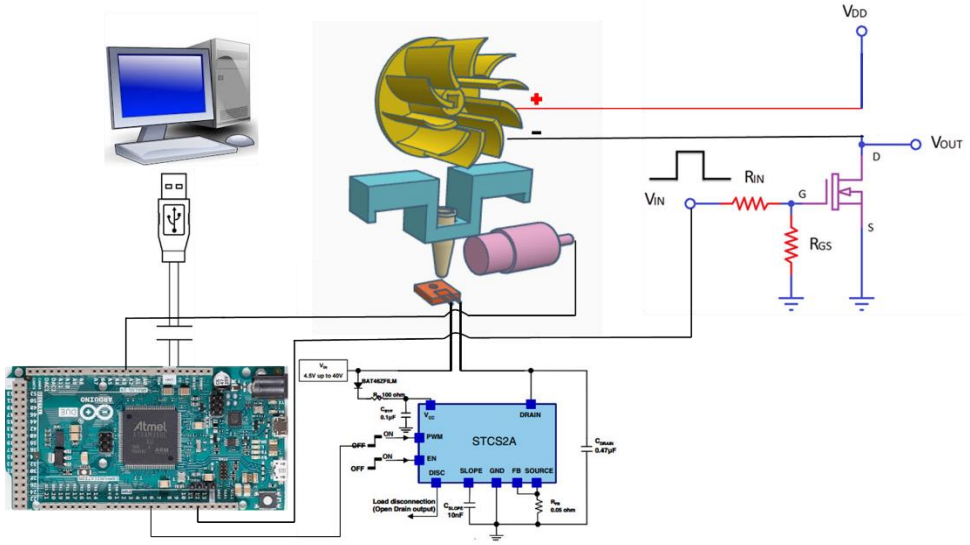

Figure 4. Design layout of VCSEL-based plasmonic thermocycler.

3. RESULTS AND DISCUSSION

3.1 VCSEL-based plasmonic thermocycler

Total reaction time for 30 cycles of PCR is achieved under ten minutes. The average of heating and cooling rates for 30 cycles are 6°C/s and 3.3°C/s respectively with driving VCSEL power less than 2W. **Figure 5** and **Figure 6** illustrate the thermocycling curve and the temperature stability of a 30 cycle PCR.

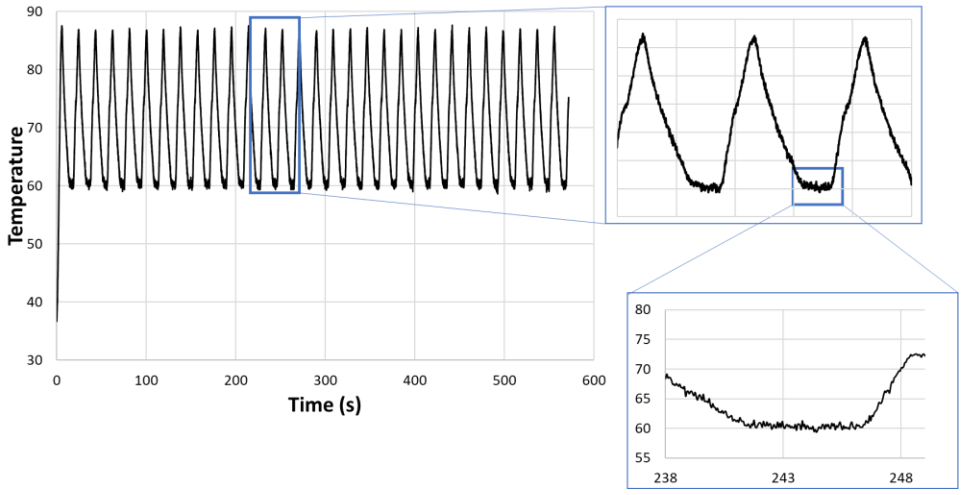

Figure 5. Thermocycling curve of 30 PCR cycles.

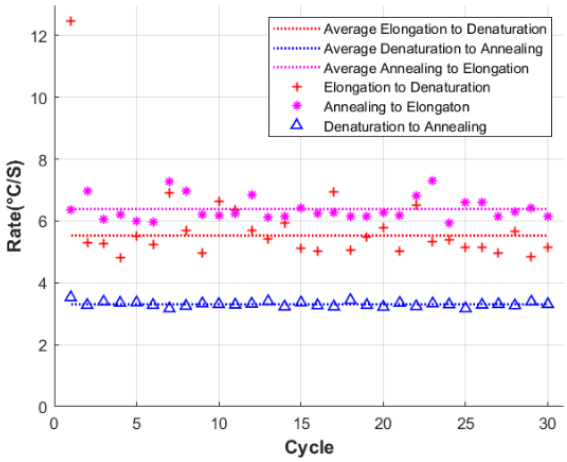

Figure 6. Heating and cooling rates.

Table 2. Mean and standard deviation of PCR temperatures, heating and cooling rates.

	Denaturation Temp. (°C)	**Annealing Temp. (°C)**	**Elongation Temp. (°C)**	**Heating rate (°C/s)**	**Cooling rate (°C/s)**
Mean	84.98	60.23	72.15	6.16	3.3
Standard deviation	0.22	0.11	0.24	0.198	0.076

To evaluate the amount and length of dsDNAs amplified by our plasmonic thermocycler, different samples with their description in **Table 3** were prepared and went through plasmonic and conventional (Eppendorf Mastercycler Nexus Thermal Cycler) PCR tests. Next, the PCR products were stained and visualized using ethidium bromide in 1% agarose gel electrophoresis under UV light. DNA ladder of size 1kb was used to identify the size of amplified DNA. **Figure 7** shows that the extended length of amplified DNA target is close to 300bp for conventional (S4) and plasmonic (S5) PCR. The VCSEL-based plasmonic thermocycler carried out the same PCR efficiency as the conventional machine in less than ten minutes. The negative controls (S1-S3) are reactions missing one of the PCR ingredients, and as a result no bands are expected on gel image. These negative controls are run along with positive controls to verify the absence of contamination introduced into the master mix or into samples. For S2, the double faint band showing small products of less than 100bp determines PCR by-product called primer dimers.

Table 3. Description of bands in gel image.

Sample No.	**Platform**	**Type of Control**
S1	Plasmonic	Negative (No DNA)
S2	Plasmonic	Negative (No Polymerase)
S3	Conventional	Negative (No DNA)
S4	Conventional	Positive
S5	Plasmonic	Positive

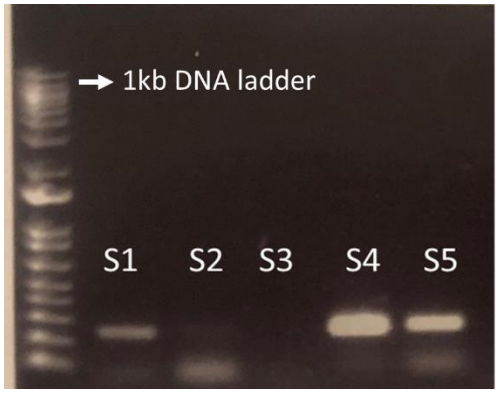

Figure 7. 1% agarose gel image of different PCR controls in VCSEL-based plasmonic and conventional thermocyclers.

3.2 Studying the inhibitory effects of excess AuNRs

Excessive concentration of AuNRs act as a PCR inhibitor due to interaction between DNA polymerase and AuNRs, and their ability to modulate the activity of polymerase [31, 32]. It has been stated that surface interaction of AuNPs mediates the enhancing effect of AuNPs in PCR rather than heat-transfer enhancement, and this leads to reduction of enzymatic activity of polymerase such as Taq in the presence of AuNPs [32, 33]. Therefore, the optimal concertation of AuNRs was investigated to fulfil the desired amplification efficiency and fast thermocycling. The stock concentration of PEG-AuNRs is 50nM and the required volume of PCR ingredients other than AuNRs and DDW is 8.4µL. Therefore, increasing the volume of AuNRs from 1 to 11.6µL and decreasing DDW's volume result in different concentrations of AuNRs in 20µL PCR solution ranging from 2.5nM to 29nM. The reactions went through conventional thermocycling, and **Figure 8** clarifies that the AuNRs' concentration can be increased to 29nM for more rapid thermocycling without any significant affinity between AuNRs and PCR ingredients. Thus, by increasing AuNRs' concentration, we can further reduce the ten-minute amplification time of the VCSEL-based thermocycler.

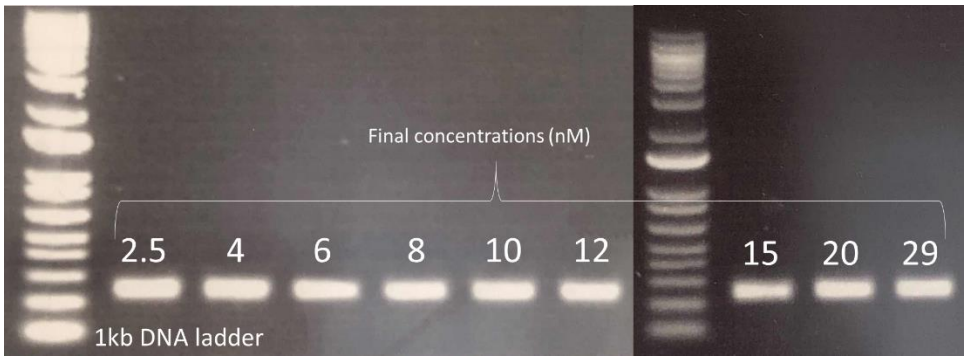

Figure 8. Comparing PCR efficiency for different AuNRs' concentration.

3.3 Analysis of relationship between AuNRs and polymerase in PCR amplification

3.3.1 UV-visible spectroscopy

To further investigate the possible interaction of AuNRs with PCR ingredients, their optical properties was monitored by UV–visible absorption spectroscopy and their size was measured by Transmission Electron Microscopy (TEM) before and after PCR. PCR reactions of positive control using different polymerases (Klentaq, KAPA2G, and Phusion) and 2.5nM AuNRs were prepared. The reactions went through conventional and plasmonic thermocycling, and the absorption of pre and post-PCR obtained by a spectrophotometer (DS-11 Series, DeNovix Inc.) were compared. **Figure 9** points out that there is no change in absorption efficiency and no spectral shift at wavelength maxima of the AuNRs for different polymerases after 40 PCR cycles. This proves that PEG-AuNRs are robust in their optical properties after prolonged CW laser irradiation in PCR solution.

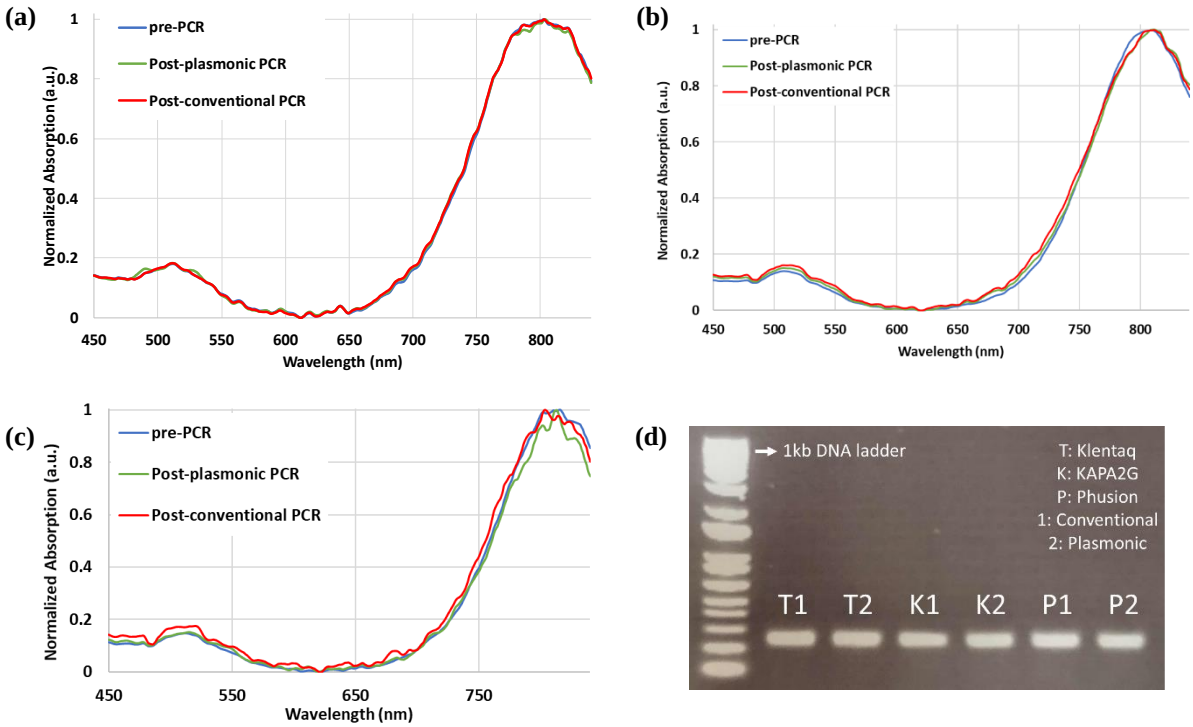

Figure 9. Normalized absorption of plasmonic PCR reaction before and after PCR with (**a**) Klentaq, (**b**) KAPA2G, and (**c**) Phusion Polymerases. (**d**) Gel image for plasmonic and conventional PCR of different polymerases.

3.3.2 Electron microscopy

Investigating AuNRs' size and their optical properties will provide us better understanding of possible interaction between PCR components and AuNRs. To verify this, reactions with positive and negative controls were prepared and underwent plasmonic PCR. 4µL drop of each sample suspension was drop cast onto a 200-mesh Cu TEM grid having carbon support film (Agar Scientific). After 60 seconds, the excess suspension was wicked off with filter paper and the grid allowed to dry under ambient conditions. The drop-cast samples were then imaged by the FEI Tecnai G2 F20 S/TEM equipped with EDAX Octane T Ultra W /Apollo XLT2 SDD and TEAM EDS Analysis System and Gatan Ultrascan 4000 4k x 4k CCD Camera System Model 895. The proprietary Gatan Digital Micrograph 16-bit images (DM3) were converted to unsigned 8-bit TIFF images (**Figure 10**). The perimeter of captured AuNRs in these TIFF images were calculated using MATLAB Image Processing Toolbox. The y-axis and x-axis in **Figure 11** represent the normalized distribution of AuNRs' perimeter (P_N) for different controls and AuNRs' perimeters in nanometers, respectively. Dense distribution is observed for AuNRs of perimeters between 100 and 150nm, while the smaller and bigger AuNRs lie in the left and right tail of normally distributed perimeter curve. The average of pre and post-PCR normalized perimeter densities ($P_{N\_average}$) were calculated and plotted in **Figure 11.e** and **Figure 11.f**, and two Gaussian curves were fitted to $P_{N\_average}$ of pre and post-PCR. The mean value of $P_{N\_average}$ for Post-PCR left shifted by 4nm and the FWHM increased by 24nm with respect to $P_{N\_average}$ for pre-PCR. The left shift and broader FWHM for post-PCR $P_{N\_average}$ indicates possible change in AuNRs' morphology as a result of thermocycling. However, this has shown no effect on optical properties of AuNRs in UV-visible spectroscopy. Therefore, this change is insignificant and dependent on the number of captured AuNRs by TEM.

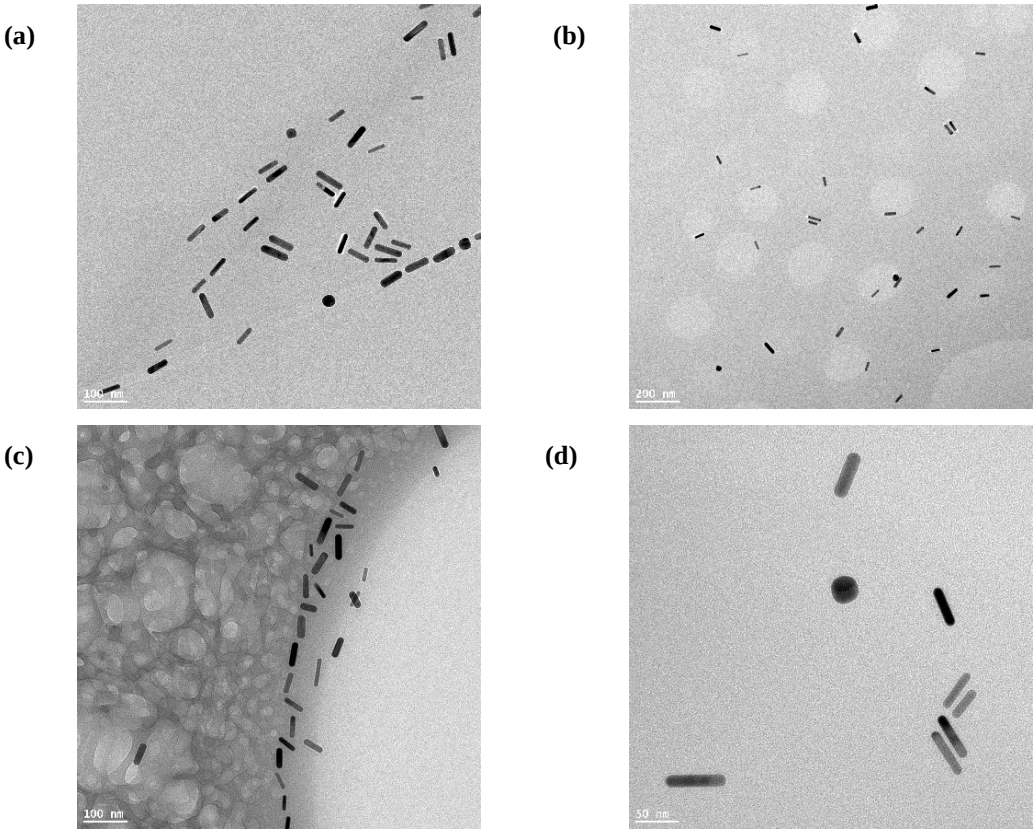

Figure 10. TEM images for (**a**) Pre-PCR positive, (**b**) Post-PCR positive (**c**) Pre-PCR negative and (**d**) Post-PCR negative controls.

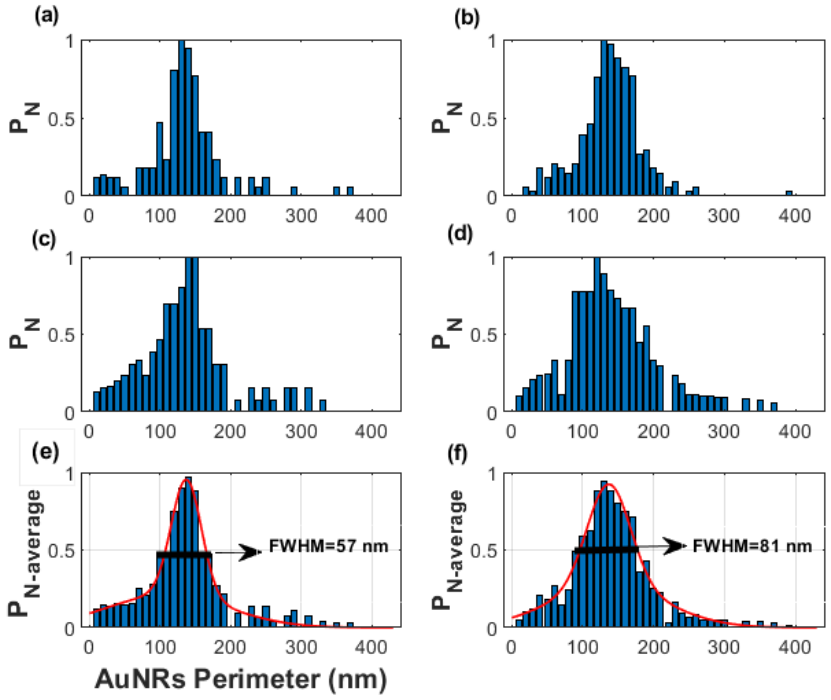

Figure 11. Calculated AuNRs' normalized perimeter densities for (**a**) Pre-PCR positive, (**b**) Post-PCR positive, (**c**) Pre-PCR negative, and (**d**) Post-PCR negative controls. Average of normalized (e) Pre-PCR and (f) post-PCR densities.

3.4 Temperature, hold-time, and heating/cooling rate Optimization

Initially, the PCR temperatures and the hold-times were set at 85°C for 1s, 60°C for 5s, and 72°C for 1s based on former plasmonic thermocyclers [26, 27]. The same temperatures demonstrate consistent and efficient PCR products in VCSEL-based thermocycler. Since a rapid thermocycler is more advantageous for POC testing, factors such as optimal annealing temperature, shorter annealing hold-time, and higher heating/cooling rate were investigated. The gel image in **Figure 12** shows that PCR fails for annealing temperatures above 60, and for hold-times less than 5s. To increase cooling rate, the input voltage was regulated to control fan's speed. Poor PCR efficiency is observed for cooling rates higher than 5°C/s. Higher cooling rates can be achieved by decreasing oil volume, as lowering the thermal mass enhances heat transfer. However, PCR failed for 25µL mineral oil. The results here reveal that there is a limit to accelerate PCR without hindering its biological and temperature-dependent reactions.

Table 4. Sample description for heating and cooling rate optimization.

Sample No.	Cooling rate (°C/s)	Annealing hold-time (s)	Annealing Temp. (°C)	Oil Volume(µL)
S1	3.3	5	60	50
S2		2.5	60	50
S3		3.5	60	50
S4		5	60	25
S5	4.1	5	60	50
S6	5	5	60	50
S7		5	63	50
S8		5	57	50

Figure 12. Gel image of sample with different cooling rates, annealing hold-time, annealing temperature, and oil volume.

Another contributing factor to faster thermocycling is the plasmonic heating rate. This was improved with increasing VCSEL's power; however, temperature control at 85 and 72°C would be a challenge for heating rates greater than 6°C/s. In other words, temperature rises above 85 and 72°C during denaturation and annealing hold-times without laser irradiation. This is due to the fact that the temperature change on the PCR plastic tube lags the temperature change of AuNRs (Thermal lag). The relaxation time for AuNRs in aqueous solution follows an approximate relationship $\tau = 0.64R(nm)^2$ dependent on AuNRs' size [34]. The effective radius ($R_{eff}=(\frac{3V}{4\pi})^{1/3}$) of the used AuNRs with volume of $3.14\times10^{-24}m^3$ is 9.08nm [35]. Thus, heat is transferred around 53ps from AuNRs of radius 9nm into the nearby water shell. However, considering the thermal resistances of PCR solution and polypropylene tube, the heat transfers from the water shell to the surface of tube significantly slower than AuNRs' relaxation time. Therefore, with increasing VCSEL's power and consequently the heating rate, this thermal lag effect accumulates, and the tube's temperature increases even when the laser is switched off and as a result no excitation in AuNRs.

3.5 Real time label-free plasmonic PCR

The VCSEL-based thermocycler was further improved by a quantitative amplicon detection system [36, 37].Since free nucleotides has the most absorbance at 260nm, their consumption during elongation stage to extend the new strand will

change the 260nm absorption of PCR solution. **Figure 13** illustrates 260nm transmission curve of a positive and negative control performed in the VCSEL-based plasmonic thermocycler. The increase in normalized UV transmission after the threshold cycle (C_t) indicates the linear amplification phase for a successful PCR. Consequently, the negative control (failed PCR) and the positive control (successful PCR) are distinguishable by the shape of transmitted UV signal.

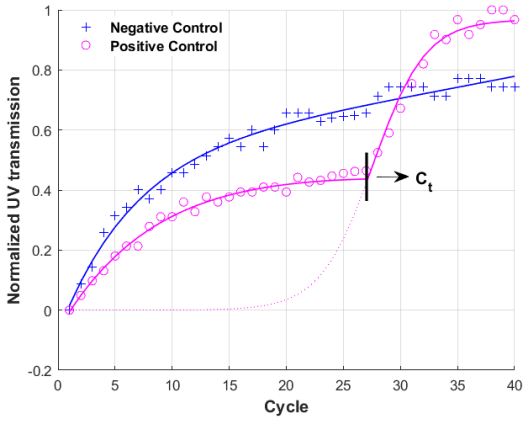

Figure 13. UV transmission curve of different PCR controls.

4. CONCLUSION

In this article, we demonstrated a novel compact rapid thermocycler through plasmonic photothermal heating of PEG-AuNRS excited by an 808nm VCSEL. The small configuration of this thermocycler was achieved via a different laser type without sample miniaturization which compromises the convenience in sample loading and the sensitivity in quantification of PCR product. Also, flexibility in positioning the light source close to PCR tube demands no light focusing components, which results in a simpler design than other proposed plasmonic thermocyclers. The amplification of 10^4 copies of *Chlamydia* DNA template with 300bp length was carried out in less than ten minutes for 30 PCR cycles. The temperature stability during hold-times and reproducibility of successful PCR results indicate the robustness of PEG-AuNRs in PCR reaction and reliability of system. The UV-visible spectroscopy of pre and post-PCR samples confirmed the unaltered optical properties of used AuNRs in our plasmonic thermocycler. Combining this portable, affordable, and low-powered VCSEL-based thermocycler with quantitative amplicon detection method delivers the same sensitivity and specificity of conventional PCR assay to POC diagnostics. The presented work can be further advanced to a multi-well plasmonic PCR on a VCSEL array to conduct multiplexed amplification and detection.

ACKNOWLEDGEMENTS

This work was supported by financial assistance of an operating grant from Genome Canada/Genome Quebec (DIG-Phase 1- 9516). Also, we thank Dr. David Liu at the Facility for Electron Microscopy Research of McGill University for help in microscope operation and data collection.

REFERENCES

[1] M. Urdea et al., "Requirements for high impact diagnostics in the developing world," Nature, vol. 444, no. Suppl 1, pp. 73-9, 2006.
[2] V. Pribul and T. Woolley, "Point of care testing," Surgery (Oxford), vol. 31, no. 2, pp. 84-86, 2013.
[3] D. Klein, "Quantification using real-time PCR technology: applications and limitations," Trends in Molecular Medicine, vol. 8, no. 6, pp. 257-260, 2002.
[4] S. Mocellin, C. R. Rossi, P. Pilati, D. Nitti, and F. M. Marincola, "Quantitative real-time PCR: a powerful ally in cancer research," Trends in molecular medicine, vol. 9, no. 5, pp. 189-95, 2003.
[5] S. A. Bustin, "REVIEW: Absolute quantification of mRNA using real-time reverse transcription polymerase chain reaction assays," Journal of molecular endocrinology., vol. 25, no. Part 2, pp. 169-193, 2000.
[6] S. A. Bustin, V. Benes, T. Nolan, and M. W. Pfaffl, "Quantitative real-time RT-PCR--a perspective," Journal of molecular endocrinology, vol. 34, no. 3, pp. 597-601, 2005.

[7] J. Engstrom-Melnyk, P. L. Rodriguez, O. Peraud, and R. C. Hein, "Clinical Applications of Quantitative Real-Time PCR in Virology," Current and Emerging Technologies for the Diagnosis of Microbial Infections, vol. 42, pp. 161-197, 2015.
[8] K. B. Mullis and F. A. Faloona, "Specific synthesis of DNA in vitro via a polymerase-catalyzed chain reaction," Methods in enzymology, vol. 155, pp. 335-50, 1987.
[9] A. B. Stephen, "How to speed up the polymerase chain reaction," Biomolecular Detection and Quantification, vol. 12, no. C, pp. 10-14. doi: 10.1016/j.bdq.2017.05.002
[10] C. D. Ahrberg, A. Manz, and B. G. Chung, "Polymerase chain reaction in microfluidic devices," Lab on a Chip, vol. 16, no. 20, pp. 3866-3884, 2016.
[11] M. U. Kopp, "Chemical Amplification: Continuous-Flow PCR on a Chip," Science, vol. 280, no. 5366, pp. 1046-1048, 1998.
[12] S. Li et al., "A Continuous-Flow Polymerase Chain Reaction Microchip With Regional Velocity Control," Journal of microelectromechanical systems : a joint IEEE and ASME publication on microstructures, microactuators, microsensors, and microsystems, vol. 15, no. 1, pp. 223-236, 2006.
[13] Q. Cao, M. C. Kim, and C. Klapperich, "Plastic microfluidic chip for continuous-flow polymerase chain reaction: simulations and experiments," Biotechnology journal, vol. 6, no. 2, pp. 177-84, 2011.
[14] T. Nakayama et al., "Circumventing air bubbles in microfluidic systems and quantitative continuous-flow PCR applications," Analytical and Bioanalytical Chemistry, vol. 386, no. 5, pp. 1327-1333, 2006.
[15] H. M. Hiep, S. Furui, Y. Yonezawa, M. Saito, Y. Takamura, and E. Tamiya, "An optimal design method for preventing air bubbles in high-temperature microfluidic devices," Analytical and Bioanalytical Chemistry, vol. 396, no. 1, pp. 457-464, 2010.
[16] P. J. Obeid and T. K. Christopoulos, "Continuous-flow DNA and RNA amplification chip combined with laser-induced fluorescence detection," Analytica Chimica Acta, vol. 494, no. 1, pp. 1-9, 2003.
[17] J. Xie, J. Shih, Q. Lin, B. Yang, and Y.-C. Tai, "Surface micromachined electrostatically actuated micro peristaltic pump," Lab on a Chip, vol. 4, no. 5, pp. 495-501, 2004.
[18] A. Brask, J. r. P. Kutter, and H. Bruus, "Long-term stable electroosmotic pump with ion exchange membranes," Lab on a Chip, vol. 5, no. 7, pp. 730-738, 2005.
[19] H. Kim, S. Vishniakou, and G. W. Faris, "Petri dish PCR: laser-heated reactions in nanoliter droplet arrays," Lab on a Chip, vol. 9, no. 9, pp. 1230-1235, 2009.
[20] T. Hideyuki et al., "Development of 1480 nm photothermal high-speed real-time polymerase chain reaction system for rapid nucleotide recognition," Japanese journal of applied physics : JJAP., vol. 47, no. 6, pp. 5212-5216, 2008.
[21] A. F. Hühmer and J. P. Landers, "Noncontact infrared-mediated thermocycling for effective polymerase chain reaction amplification of DNA in nanoliter volumes" Analytical chemistry, vol. 72, no. 21, pp. 5507-12, 2000.
[22] A. St John and C. P. Price, "Existing and Emerging Technologies for Point-of-Care Testing," The Clinical biochemist. Reviews, vol. 35, no. 3, pp. 155-67, 2014.
[23] J. H. Son et al., "Ultrafast photonic PCR," Light: Science & Applications, vol. 4, no. 7, pp. e280-e280, 2015/07/01 2015.
[24] P. J. Roche et al., "Demonstration of a plasmonic thermocycler for the amplification of human androgen receptor DNA," The Analyst, vol. 137, no. 19, pp. 4475-81, 2012.
[25] P. J. R. Roche et al., "Real time plasmonic qPCR: how fast is ultra-fast? 30 cycles in 54 seconds," The Analyst, vol. 142, no. 10, pp. 1746-1755, 2017.
[26] G. Uchehara, A. G. Kirk, M. Trifiro, M. Paliouras, and P. Mohammadyousef, "Real time label-free monitoring of plasmonic polymerase chain reaction products," in Nano-, Bio-, Info-Tech Sensors and 3D Systems III 2019, March 4, 2019 - March 6, 2019, Denver, CO, United states, 2019, vol. 10969, pp. OZ Optics, Ltd.; Polytec, Inc.; The Society of Photo-Optical Instrumentation Engineers (SPIE): SPIE.
[27] N. A. M. Tran, "Universal point of care biosensor using ultrafast plasmonic polymerase chain reaction," McGill University Libraries, [Montreal], 2019.
[28] J. Kim, H. Kim, J.-H. Park, and S. Jon, "Gold Nanorod-based Photo-PCR System for One-Step, Rapid Detection of Bacteria," Nanotheranostics, vol. 1, pp. 178-185, 05/06 2017.
[29] S. Li, Y. Gu, Y. Lyu, Y. Jiang, and P. Liu, "Integrated Graphene Oxide Purification-Lateral Flow Test Strips (iGOP-LFTS) for Direct Detection of PCR Products with Enhanced Sensitivity and Specificity," Analytical chemistry, vol. 89, no. 22, pp. 12137-12144, 2017.

[30] S. Gilbert et al., "Increased sample volume and use of quantitative reverse-transcription PCR can improve prediction of liver-to-blood inoculum size in controlled human malaria infection studies," Malaria Journal, vol. 14, no. 1, pp. 1-9. doi: 10.1186/s12936-015-0541-6
[31] L. Mi, H. Zhu, X. Zhang, J. Hu, and C. Fan, "Mechanism of the interaction between Au nano-particles and polymerase in nanoparticle PCR," Chinese Science Bulletin, vol. 52, no. 17, pp. 2345-9, 2007.
[32] S. Mandal, M. Hossain, T. Muruganandan, G. S. Kumar, and K. Chaudhuri, "Gold nanoparticles alter Taq DNA polymerase activity during polymerase chain reaction," RSC Advances, vol. 3, no. 43, pp. 20793-20799, 2013.
[33] B. V. Vu, D. Litvinov, and R. C. Willson, "Gold Nanoparticle Effects in Polymerase Chain Reaction: Favoring of Smaller Products by Polymerase Adsorption," Analytical Chemistry, vol. 80, no. 14, pp. 5462-5467, 2008/07/01 2008.
[34] M. Hu and G. V. Hartland, "Heat Dissipation for Au Particles in Aqueous Solution: Relaxation Time versus Size," The journal of physical chemistry. B, Condensed matter, materials, surfaces, interfaces & biophysical., vol. 106, no. 28, p. 7029, 2002.
[35] K. Park, S. Biswas, S. Kanel, D. Nepal, and R. A. Vaia, "Engineering the Optical Properties of Gold Nanorods: Independent Tuning of Surface Plasmon Energy, Extinction Coefficient, and Scattering Cross Section," The Journal of Physical Chemistry C, vol. 118, no. 11, pp. 5918-5926, 2014.
[36] P. Mohammadyousef, M. Trifiro, M. Paliouras, and A. G. Kirk, "Ultrafast plasmonic and real-time label-free polymerase chain reaction," in SPIE BiOS, San Francisco, California United States, 2020: SPIE International Society for Optics and Photonics.
[37] M. Tran, M. Paliouras, P. Mohammadyousef, M. Trifiro, and A. G. Kirk, "Real-time fluorophore-free optical monitoring of ultrafast DNA amplification for qPCR," presented at the 2nd European Biosensor Symposium 2019, EBS2019, Florence, Italy, 2019.